Computer-Controlled Mechanical Simulation of the Artificially Ventilated Human Respiratory System

Samir Mešić, Robert Babuška*, Henk C. Hoogsteden, and Anton F. M. Verbraak

***Abstract*—A mechanical lung simulator can be used to simulate specific lung pathologies, to test lung-function equipment, and in instruction. A new approach to mechanical simulation of lung behavior is introduced that uses a computer-controlled active mechatronic system. The main advantage of this approach is that the static and dynamic properties of the simulator can easily be adjusted via the control software. A nonlinear single-compartment mathematical model of the artificially ventilated respiratory system has been derived and incorporated into the simulator control system. This model can capture both the static and dynamic compliance of the respiratory system as well as nonlinear flow-resistance properties. Parameters in this model can be estimated by using data from artificially ventilated patients. It is shown that the simulation model fits patient data well. This mathematical model of the respiratory system was then matched to a model of the available physical equipment (the simulator, actuators, and the interface electronics) in order to obtain the desired lung behavior. A significant time delay in the piston motion control loop has been identified, which can potentially cause oscillations or even instability for high compliance values. Therefore, a feedback controller based on the Smith-predictor scheme was developed to control the piston motion. The control system, implemented on a personal computer, also includes a user-friendly interface to allow easy parameter setting.**

***Index Terms*—Artificial ventilation, computer-controlled system, dynamic compliance, mechanical simulation, modeling, parameter estimation, Smith predictor.**

NOMENCLATURE

COPD	Chronical obstructive pulmonary disease.
C	Compliance of the respiratory system [lkPa^{-1}].
C_L	Lung compliance [lkPa^{-1}].
$C_{\rm th}$	Thorax compliance [lkPa^{-1}].
DMC	Digital motion controller.
E	Total lung elasticity [l^{-1}kPa].
E_a	Elasticity of the air [l^{-1}kPa].
E_m	Elasticity of the Maxwell body [l^{-1}kPa].
F	Measured air flow [ls^{-1}].
FRC	Functional residual capacity [l].
GBN	Generalized binary noise.
K_1	Viscosity ratio coefficient [–].
K_F	Flow resistance coefficient [kPas^{2}l^{-2}].
K_V	Volume resistance coefficient [kPasl^{-2}].
$\mathrm{LamW}(x)$	Lambert's W function.
m_a	Mass of the air [kg].
P_A	Alveolar pressure [kPa].
$P_{\rm aw}$	Pressure exerted in the airways [kPa].
PEEP	Positive end expiratory pressure [kPa].
P_L	Elastic recoil pressure [kPa].
P_m	Mouth pressure [kPa].
$P_{\rm mus}$	Pressure exerted by the muscles [kPa].
$P_{\rm pl}$	Intrapleural pressure [kPa].
$P_{\rm th}$	Thorax recoil pressure [kPa].
$P_{\rm tr}$	Tracheal pressure [kPa^{-1}].
R	Airway resistance [kPasl^{-1}].
R_0	Laminar flow resistance [kPasl^{-1}].
R_a	Air resistance [kPasl^{-1}].
R_m	Resistance of the Maxwell body [kPasl^{-1}].
τ_1	Time constant due to fast changes in the lung volume [s].
τ_2	Time constant due to viscosity [s].
T_{dv}	Time delay in the piston control loop [s].
TLC	Total lung capacity [l].
T_s	Sample time [s].
V	Lung volume increment above FRC [l].
V_L	Lung volume [l].
$V_{\rm ref}$	Volume reference [l].
x	Sleeve position [–].
$x_{\rm ref}$	Sleeve position reference [–].

Manuscript received July 11, 2002. *Asterisk indicates corresponding author*.

S. Mešić is with the Delft Center for Systems and Control, Delft University of Technology, 2628 CD Delft, The Netherlands, and also with the Department of Pulmonary Diseases, Erasmus University Medical Center, 3015 GD Rotterdam, The Netherlands.

*R. Babuška is with the Delft Center for Systems and Control, Delft University of Technology, Mekelweg 2, 2628 CD Delft, The Netherlands (e-mail: R.Babuska@dcsc.tudelft.nl).

H. C. Hoogsteden and A. F. M. Verbraak are with the Department of Pulmonary Diseases, Erasmus University Medical Center, 3015 GD Rotterdam, The Netherlands.

Digital Object Identifier 10.1109/TBME.2003.812166

I. INTRODUCTION

ALTHOUGH MECHANICAL ventilation is normally regarded as a rescue therapy, there are many patients who require long-term ventilatory support. A sophisticated mechanical simulator can be used to simulate a broad spectrum of lung pathologies in order to test the lung-function equipment and software. It is also useful for research purposes and instruction in a real physical environment.

The starting point of this research was an existing mechanical simulator including the necessary sensors, actuators, interface electronics, and local controllers. The main component of the simulator is an air compartment with a piston driven by an electrical motor. By controlling the piston motion, one can simulate the alveolar space and the elastance of the respiratory system. The air outlet is connected to a computer-controlled adjustable flow resistor to simulate the airways resistance.

The goal was to develop a computer-based control system that actively controls the simulator such that it approximates a prescribed behavior of an artificially ventilated human respiratory

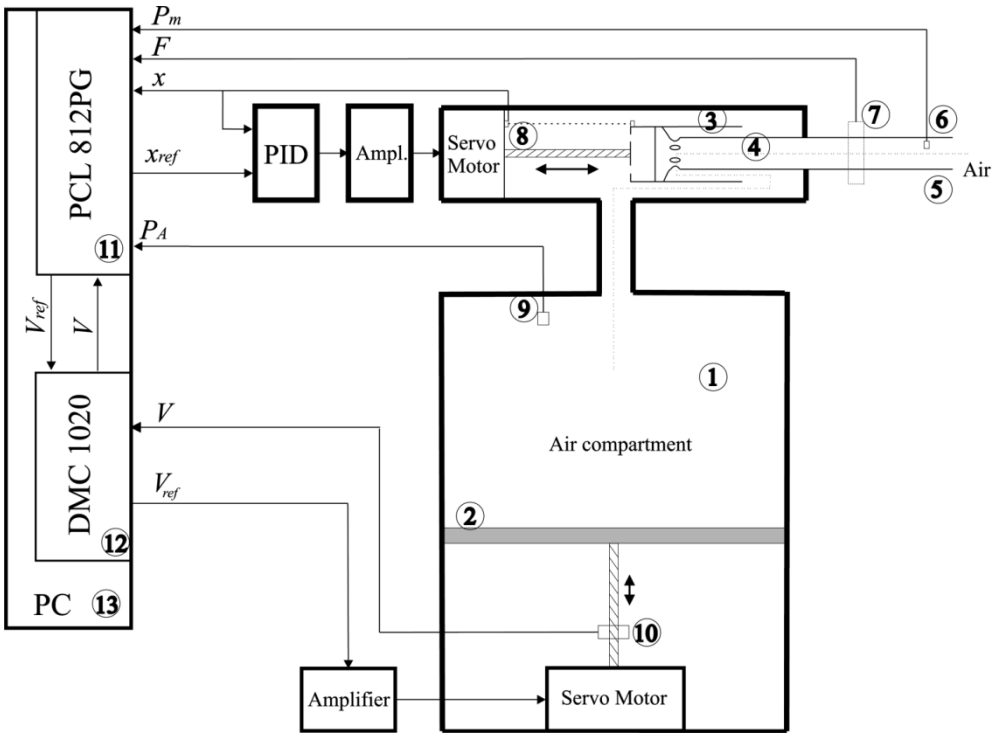

Fig. 1. Mechanical lung simulator with the sensors, actuators, electronic interfaces, and controllers. (1) Air compartment. (2) Piston. (3) Resistance sleeve. (4) Resistance cylinder. (5) Air outlet. (6) Mouth pressure sensor. (7) Flow sensor. (8) Sleeve position sensor. (9) Compartment pressure sensor. (10) Piston position encoder. (11) Interface card. (12) DMC. (13) PC.

system. To achieve this goal, one needs to develop two models and a control system.

1) *A mathematical model of the respiratory system to be simulated*. In order to exploit the full potential of the simulator, we developed a flexible nonlinear dynamic model that includes various aspects of lung behavior. Effects such as nonlinear static compliance [1] and viscoelasticity [2], [3] have been incorporated. As models published in the literature [4]–[7], turned out to be not completely suitable for this purpose, we developed a new model and implemented it in MATLAB/Simulink. A procedure was designed to estimate the parameters of this model by using data from artificially ventilated patients.
2) *A mathematical model of the mechanical simulator (physical equipment)*. This model is clearly different from the one above, as it describes the dynamic behavior of the physical equipment and not the lungs. The model includes dynamic submodels for the air compartment and the adjustable resistor. Based on this model, a controller can be designed such that the desired behavior defined by the above model of the respiratory system can be simulated.
3) *A control system that actively drives the actuators such that the simulator behaves like the prescribed mathematical model of the lungs*. As the properties of the mechanical system naturally differ from those of the human lungs, this control system is essential for achieving the desired compliance properties, nonlinearities, volume, and flow-dependent characteristics, etc. It also has to compensate for parasitic phenomena such as time delays in the control loops and (undesired) nonlinearities of the simulator itself.

The rest of this paper is organized as follows: Section II describes the computer-controlled lung simulator. In Section III, the mathematical model of the human respiratory system is derived, while Section IV addresses the modeling and identification of the lung simulator. In Section V, the control design, implementation and real-time results are described. Section VI concludes the paper.

II. Description of the Simulator Setup

Fig. 1 gives a schematic representation of the mechanical system together with the actuators, interface electronics, low-level position controllers, and the control computer.

The air compartment [Fig. 1(1)] with the piston [Fig. 1(2)] simulates the alveolar space and the elastance of the respiratory system. The minimum volume inside the compartment is 1.77 L and the maximum volume is 5.38 L. The piston is driven by a servo motor via a screw and its motion dynamically changes the volume inside the compartment. The piston position is measured using an encoder [Fig. 1(10)] and it is controlled by the DMC 1020 [8].

The outlet of the compartment is connected to an adjustable flow resistor which consists of a cylinder [Fig. 1(4)] surrounded by a sleeve [Fig. 1(3)]. The air flows through eight holes symmetrically arranged around the circumference of the cylinder into a narrow space (slit) between the outer side of the cylinder and the inner side of the sleeve. This space is called the active resistance region. The position x of the sleeve can be adjusted by means of a servo motor, thereby changing the length of the slit and, thus, the flow resistance. The internal diameter of the

sleeve is 33.98 mm (different resistance ranges can be obtained by using cylinders with different diameters).

A potentiometer [Fig. 1(8)] measures the actual position of the sleeve, which is normalized into the real interval $[-1, 0]$. When the sleeve is open (extreme left position), the flow resistance is minimal $(x = 0)$. When the sleeve is at its extreme right position, the flow resistance is maximal $(x = -1)$. The main construction goal for the flow resistance was to achieve a laminar flow of the air in the active resistance region (the resistance R then has a linear relationship to the sleeve position x). However, due to the relatively high flow rate and gas acceleration, turbulence effects are present. A more detailed description of the mechanical simulator is given in [9] and [10].

Pressure sensors measure the "mouth" pressure [Fig. 1(6)] and the compartment pressure [Fig. 1(9)]. The flow F is measured as the pressure drop over a low resistance [Fig. 1(7)] inside the outlet [Fig. 1(5)]. The Advantech personal computer (PC) lab card PCL812 [Fig. 1(11)] converts the analog input signals P_A, x, F, P_m, and V into a digital form and generates the analog output signals: the volume reference V_{ref} and the sleeve position reference x_{ref} [11].

The real-time controller of the entire system has been implemented in MATLAB 6.0/Simulink 4.0 (The MathWorks Inc., Natick, USA) installed on a PC (Pentium 800 MHz running Windows 95). MATLAB communicates with the interface card PCL812 PG by using the Real-Time Toolbox (version 3.0) and with the DMC through a Windows application written in Delphi (using the Delphi Galil DMC components [8]). To implement this communication, MATLAB's dynamic data exchange functions are used.

The photograph in Fig. 2 shows the complete setup. At the top of the simulator, one can see the computer-controlled flow resistance [Fig. 2(a)] which simulates the airways resistance. The air compartment [Fig. 2(d)] is partly visible behind the monitor [Fig. 2(f)].

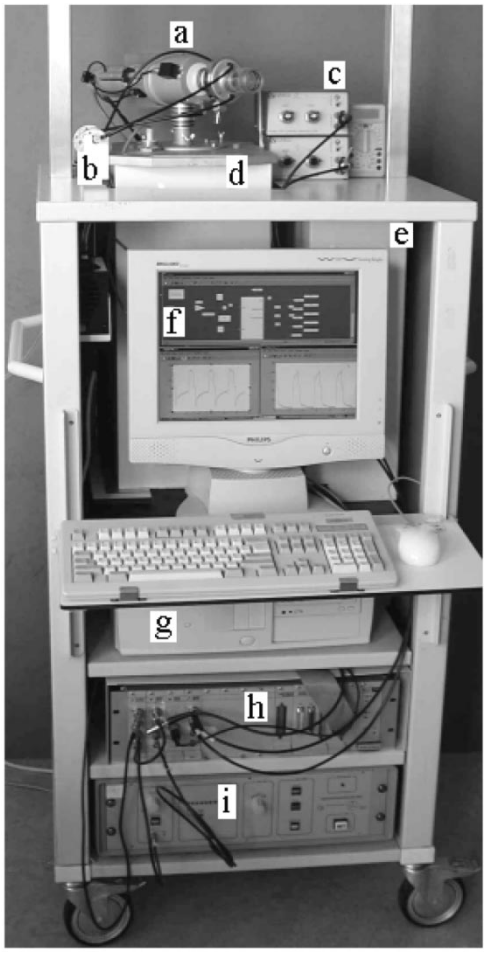

Fig. 2. Photograph of the lung simulator including the PC for real-time data acquisition and control. (a) Air resistor. (b) Pressure sensors. (c) Pressure transducers. (d) Compartment space. (e) Piston power electronics. (f) Monitor. (g) PC. (h) PCL812 PG interface electronics. (i) Resistor power electronics and control system.

III. Mathematical Model of the Human Respiratory System

The human respiratory system consists of the lungs, conducting airways, pulmonary vasculature, respiratory muscles, and surrounding tissues and structures [12]–[14] (see Fig. 3). It is a dynamic, nonlinear [15], nonstationary, distributed-parameters system that is to some extent stochastic. Physical modeling [4], [5] and the use of empirical formulas in combination with data fitting [6], [7], [16] constitute the common approaches to human respiratory system modeling.

The simplest model of the respiratory system is the following linear single-compartment model [17]:

$$P_m(t) = EV(t) + R\dot{V}(t) \tag{1}$$

where P_m is the airways opening (mouth) pressure, E is the lumped elastance of the lung and thorax, and R is the resistance of the airways. The air flow is approximated by the volume derivative with respect to time, $\dot{V}(t)$. Air compression is neglected in this model, which is common practice [4]–[7]. However, the relationship between the compliance and other respiratory system variables such as the volume and the alveolar pressure is generally dynamic and nonlinear. This section describes an extension and implementation of the above single-compartment model. Nonlinear static compliance, linear

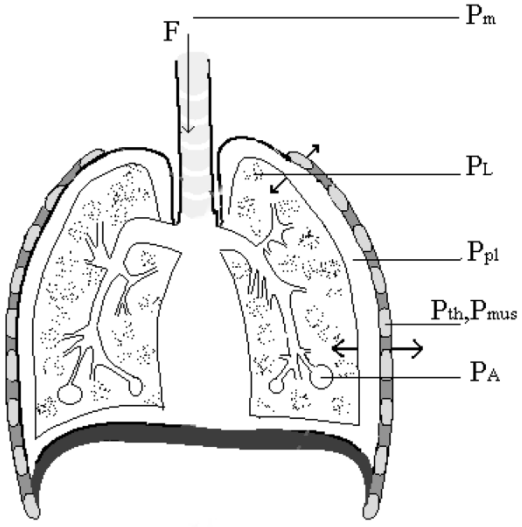

Fig. 3. Schematic representation of the respiratory system.

dynamic compliance, and nonlinear air resistance are integrated in this new model.

A. Nonlinear Static Compliance

Nonlinear static compliance [1] is included in the model because the simulator can be used over a large volume range. The compliance C of the respiratory system is defined as the change of the lung volume per unit change in the alveolar pressure

$$C = \frac{1}{E} = \frac{\Delta V_L}{\Delta P_A}. \tag{2}$$

The total compliance of the respiratory system consists of the lung compliance and the thorax compliance. The lung compliance can be described as a static volume-pressure characteristic, given by the following empirical equation [1]:

$$V_L = \mathrm{TLC}\left(1 - e^{-\frac{P_L - P_0}{P_{\mathrm{tr}}}}\right). \tag{3}$$

Here, TLC is the total lung capacity, P_{tr} is the tracheal pressure, and P_0 is the pressure at $V_L = 0$. The elastic behavior of the chest wall (thorax) is determined by the chest wall compliance C_{th} [18]

$$V_L = C_{\mathrm{th}} P_{\mathrm{th}} + 0.8\mathrm{TLC}. \tag{4}$$

The volume at which the pressures of the lung and the thorax are of equal amplitude and opposite sign is known as the FRC. The following relations hold for the intrapleural pressure P_{pl} [10]:

$$P_{\mathrm{pl}} = P_A - P_L, \tag{5}$$

$$P_{\mathrm{pl}} = P_{\mathrm{th}} + P_{\mathrm{mus}} \tag{6}$$

where P_A is the alveolar pressure and P_{mus} is the pressure exerted by the muscles. In artificially ventilated patients, the muscular activities are suppressed; thus, $P_{\mathrm{mus}} = 0$, which gives

$$P_A = P_L + P_{\mathrm{th}}. \tag{7}$$

By expressing the pressures from (3) and (4) and substituting them into (7), we obtain the following nonlinear equation for the alveolar pressure:

$$P_A = \frac{V_L - 0.8\mathrm{TLC}}{C_{\mathrm{th}}} - P_{\mathrm{tr}} \ln\left(\frac{\mathrm{TLC} - V_L}{\mathrm{TLC}}\right) + P_0. \tag{8}$$

As this relation is monotonic in V_L, the inverse function $V_L = g(P_A)$ exists, although it is rather complex

$$\begin{aligned} V_L = {} & P_A C_{\mathrm{th}} + 0.8\mathrm{TLC} + P_{\mathrm{tr}} C_{\mathrm{th}} \\ & \times \ln\left[\frac{P_{\mathrm{tr}} C_{\mathrm{th}}}{\mathrm{TLC}} \mathrm{LamW}\left(\frac{\mathrm{TLC}}{P_{\mathrm{tr}} C_{\mathrm{th}}} e^{\frac{0.2\mathrm{TLC} + P_0 C_{\mathrm{th}} - P_A C_{\mathrm{th}}}{P_{\mathrm{tr}} C_{\mathrm{th}}}}\right)\right] \\ & - P_0 C_{\mathrm{th}}. \end{aligned} \tag{9}$$

Here, $w = \mathrm{LamW}(x)$ is the Lambert's W function [19], i.e., the solution to $we^w = x$. To keep the presentation simple, in the sequel, we will consider that (9) is linearized at the operating point $P_A = 0$ and $V_L = \mathrm{FRC}$, which yields the standard affine model

$$V_L = \frac{1}{E} P_A + \mathrm{FRC}. \tag{10}$$

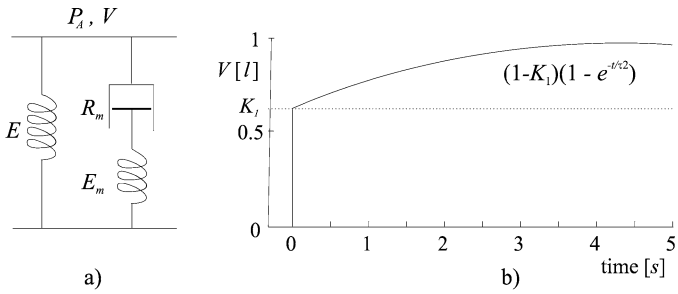

Fig. 4. (a) Viscoelastic model with elastance E for the respiratory system, and elastance E_m and resistance R_m for the Maxwell body. (b) Volume V as a function of time after a step change $\Delta P_A = 1$ kPa (see also [2]).

Due to the tissue properties of the lung and thorax, the compliance of the respiratory system cannot be described solely by the above static relationships. A dynamic model is, therefore, derived in the following section.

B. Dynamic Compliance

Dynamic effects can be modeled by incorporating viscoelasticity [2], [20], [21] or plastoelasticity [22], [23]. Fig. 4 presents a standard mechanical model with elastic and viscoelastic elements [2]. The viscoelastic effects are modeled as a Maxwell body, parallel to the elasticity E of the respiratory system (linear, for the simplicity of notation). The Maxwell body [3], [4] consists of an elastic element E_m in series with a viscous element R_m.

The viscoelastic model can be approximated by a second-order linear model. We propose the following weighted parallel connection of two first-order systems:

$$G_V(s) = \frac{V(s)}{P_A(s)} = \frac{1}{E}\left[K_1 G_{V1}(s) + (1 - K_1) G_{V2}(s)\right] \tag{11}$$

with $K_1 \in (0, 1)$ and

$$G_{V1}(s) = \frac{1}{\tau_1 s + 1}, \quad G_{V2}(s) = \frac{1}{\tau_2 s + 1}.$$

The time constant τ_1 represents the fast (almost abrupt) change in the lung volume due to lung elasticity and τ_2 the slow change due to viscosity. According to Fig. 4, when τ_1 tends to zero, K_1 and τ_2 are given by

$$K_1 = \frac{E}{E + E_m}, \quad \tau_2 = \frac{R_m(E + E_m)}{E E_m}. \tag{12}$$

C. Airways Resistance

The airways resistance is the ratio of the pressure loss in the airways to the flow rate

$$R = \frac{P_{\mathrm{aw}}}{\dot{V}}. \tag{13}$$

The upper-airways resistance is modeled as flow dependent, the resistance of the small airways is assumed to be constant, and the resistance of those airways generations which are susceptible to changes in the lung pressure is assumed to be volume dependent [5], [14]. The following equation is used in our research to represent the volume and flow dependence:

$$R = R_0 + K_V V + K_F |\dot{V}|. \tag{14}$$

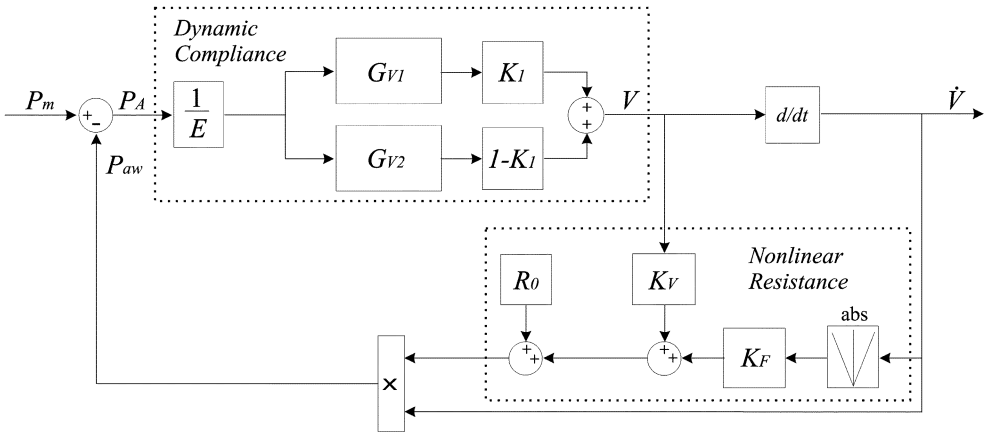

Fig. 5. Complete model of the respiratory system.

This model can be extended to incorporate other aspects of airways resistance, such as different parameter values for inspiration and expiration [7], [24].

D. The Complete Model and Its Validation

The alveolar pressure P_A equals the pressure at the mouth P_m decreased by the pressure drop due to the airways resistance P_{aw}

$$P_A = P_m - P_{\text{aw}}. \tag{15}$$

Using the dynamic compliance model (11) and the airways resistance model (14), we obtain the complete model depicted in Fig. 5. Although this model can be expressed in terms of differential equations, for the purpose of control design it is more convenient and instructive to keep it as a block diagram. Note also that the constant compliance $1/E$ can be replaced by the nonlinear function (9).

To validate this model, we estimated its parameters by using real data from artificially ventilated patients and compared the simulated time response with the measured one. For the sake of space, we only show results for one patient data set (fibrotic lungs). The same approach, however, can be applied to data of patients with other pathologies, see, e.g., [25], where 15 patient data sets were used (five fibrosis patients, five with emphysema, and five with normal lungs).

The pressure at the mouth P_m and the flow rate F were sampled at 100 Hz. The data sequence length was 3000 samples (30 s). After removing linear trends from the flow-rate data, we computed the volume by numerically integrating the flow rate. The estimation procedure consists of two steps.

1) First, initial values of parameters E, R_0, K_V, and K_F were estimated by applying the least-squares method to the following simplified model that only includes the static compliance and the airways resistance:

$$P_m = EV + \left(R_0 + K_V V + K_F|\dot{V}|\right)\dot{V}.$$

This model is linear in all its parameters and, therefore, a globally optimal parameter estimate is obtained. Initial values for K_1 and τ_2 were obtained from the literature [2]. The fast time constant τ_1 was chosen sufficiently small with respect to τ_2.

2) These parameters were used as an initial guess for nonlinear least-squares optimization. The Levenberg–Marquardt method [26], [27] was applied to the complete model of Fig. 5 with the objective to minimize the sum of squared differences between the measured and simulated flow rate. The mouth pressure P_m was used as an input to the model. Fig. 6 shows a typical example of a breathing cycle measured in a flow-ventilated fibrosis patient. During inspiration, the flow delivery system creates a positive pressure P_m and constant flow F in the tube connected to the patient's airways. After the inspiration phase, there is a respiratory pause during which the outlet valve of the tube is closed, keeping the flow equal to zero. This makes the gas exchange process in the patient's lungs more effective. The expiration is passive, i.e., the valve is open and the air is forced out of the lungs due to the elastic contraction of the lungs and the chest wall. The simulated flow is shown as the dotted line. One can see that the measured and the simulated flow are in a good agreement. Table I gives the initial and final parameters obtained for this patient according to the above procedure.

IV. Modeling and Identification of the Lung Simulator

The mathematical model of the lung, given in Fig. 5, describes the desired dynamic behavior that the mechanical simulator should exhibit. However, without proper control, the actual behavior of the simulator is quite different from the desired one (e.g., it cannot represent lung compliance, elasticity, or particular nonlinearities). Therefore, it is necessary to design a control system to obtain the desired dynamic properties (in other words, to make the hardware components of the simulator behave like the corresponding elements of the lung mathematical model).

To facilitate the controller design, we need an accurate model of the mechanical simulator, including the electronic interfaces. This model also has to capture parasitic phenomena inherent to the mechanical simulator setup, such as time delays in the control loops and undesired nonlinearities of the simulator itself. In the sequel, we describe the modeling and identification of the dynamic and static characteristics of the flow resistor and of the piston motion.

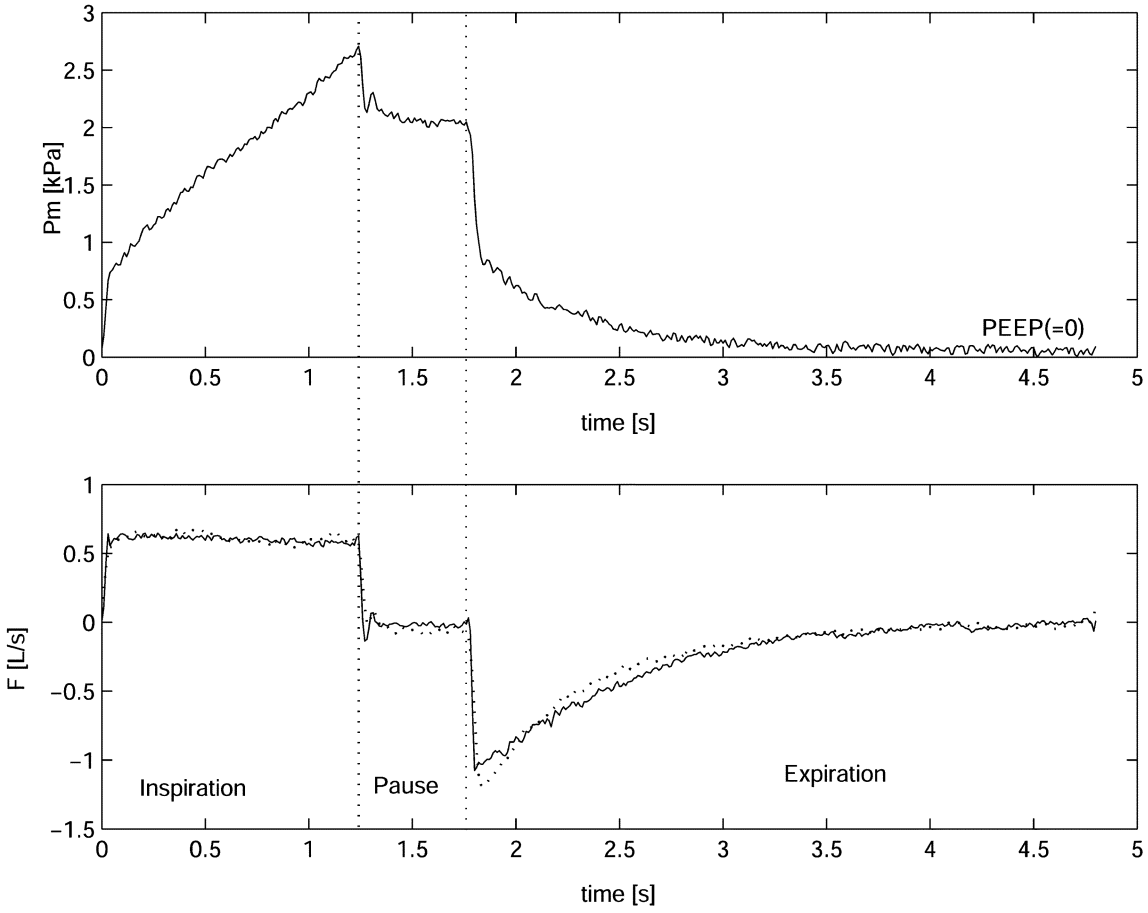

Fig. 6. Mouth pressure and flow recorded in a fibrotic patient (solid lines) and flow simulated by the model of Fig. 5 (dotted line). No PEEP is present.

TABLE I
INITIAL AND FINAL PARAMETER VALUES FOR THE RESPIRATORY SYSTEM MODEL

Parameter	Unit	Initial value	Final value
E	kPa l^{-1}	2.59	2.37
R_0	kPa s l^{-1}	1.02	0.47
K_V	kPa s l^{-2}	-0.17	-0.45
K_F	kPa s^{2}l^{-2}	0.13	0.01
K_1	–	0.75	0.83
τ_2	s	5.27	3.89
τ_1	s	0.10	0.26

A. Computer-Controlled Flow Resistance

The sleeve position, which determines the flow resistance of the computer-controlled resistor, is controlled by a proportional-integral-derivative (PID) controller with fixed parameters, using the scheme depicted in Fig. 7. This controller is connected to the PC through an analogue interface of the PCL 812PG card (see also Fig. 1). The resistance is a nonlinear function of the sleeve position and the flow [9]. The identification of this subsystem, thus, comprises the identification of the sleeve-position closed-loop dynamics G_x and the static nonlinearity $f(x, F)$.

The transfer function G_x was determined in the *discrete time domain* by means of system identification. The reference input $x_{\rm ref}$ was excited by a pseudorandom binary signal. The sampling rate was 200 Hz and the experiment duration 30 s. The following transfer function was obtained by using the output-error method [28]

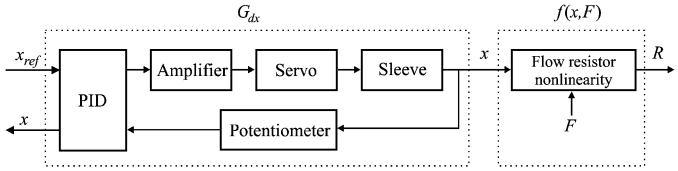

Fig. 7. Sleeve position control loop and resistor nonlinearity.

$$G_{dx}(q) = \frac{X(q)}{X_{\rm ref}(q)} = G_x(q)\frac{1}{q^5} = \frac{0.0021q + 0.0013}{(q^3 - 2.7065q^2 + 2.4682q - 0.7583)q^5}. \quad (16)$$

The time delay of five samples (corresponding to 0.025 s) is due to the interface electronics and the software.

The static nonlinearity $R = f(x, F)$ was described in a lookup table, by measuring the resistance at different flow rates and different (steady-state) sleeve positions. A graph of this table for the cylinder diameter 33.20 mm is shown in Fig. 8.

B. Air-Compartment Dynamics

The piston position, which determines the volume inside the compartment, is controlled by a PID controller with fixed pa-

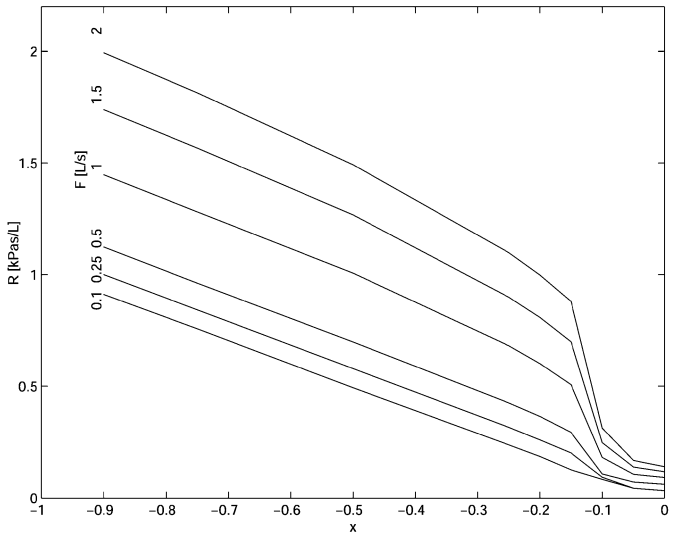

Fig. 8. Flow resistance R as a function of the sleeve position x and the flow F.

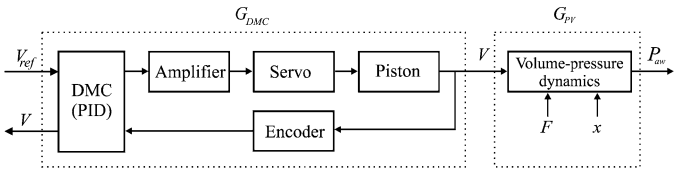

Fig. 9. Piston-position control loop and volume-pressure dynamics.

rameters, using the scheme depicted in Fig. 9. This controller is implemented in the DMC and it is connected to the PC through an analogue interface of the PCL 812PG card (see also Fig. 1). In addition to the piston-position closed-loop dynamics $G_{\rm DMC}$, the volume-pressure dynamics $G_{\rm PV}$ (due to air compression and transport) must be modeled.

The DMC is programmed such that the closed loop approximates a linear first-order system with a time constant of 0.1 s. This value has been chosen as it is the shortest possible time constant that can be achieved with the given hardware and software. In order to obtain a more accurate model of the closed loop, we identified a third-order transfer function $G_{\rm DMC}$ in the discrete-time domain by using the output-error method. Again, a pseudorandom binary input signal was applied to excite the input $V_{\rm ref}$. The sampling rate was 200 Hz and the experiment duration 30 s. The following transfer function was obtained:

$$G_{\rm dDMC}(q) = \frac{V(q)}{V_{\rm ref}(q)} = G_{\rm DMC}(q)\frac{1}{q^5} = \frac{0.0150q - 0.0125}{(q^3 - 2.6251q^2 + 2.3167q - 0.6891)q^5}. \quad (17)$$

Note the time delay of five samples (corresponding to 0.025 s), which is due to the interface electronics and the software.

While in the mathematical model of the lungs, air compression is usually neglected (see Section III), in a control-oriented model of the mechanical system, it is important to capture the dynamics as accurately as possible. To model the air compression, we use a mechanical analogue consisting of a spring, a mass, and a friction element (see Fig. 10).

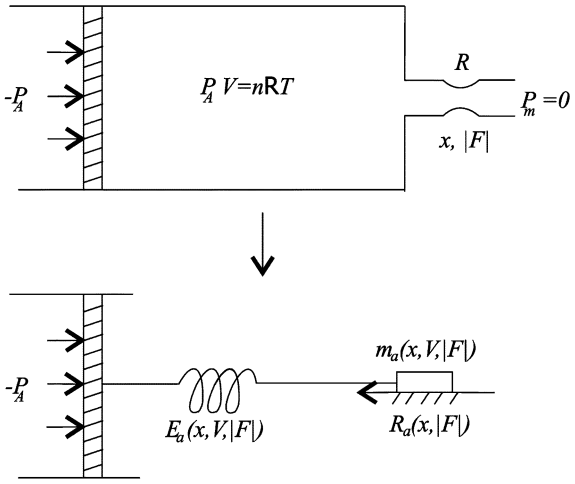

Fig. 10. Mechanical analogue to model the pressure in the compartment as a result of air compression and flow resistance.

TABLE II
THE MODELING ACCURACY OF $G_{\rm PV}$ AT 24 OPERATING POINTS

V\x	-0.10	-0.15	-0.20	-0.50	-0.75	-0.90
2.0	93.9%	93.7%	93.5%	93.8%	93.9%	93.5%
2.5	93.8%	93.6%	93.4%	94.0%	94.0%	94.5%
3.0	93.9%	93.7%	93.5%	94.1%	94.2%	95.4%
3.5	94.0%	93.7%	93.5%	94.0%	93.9%	95.8%

A sudden negative change of volume causes air compression in the compartment and outflow of the air. In Fig. 10, the compression is represented by the spring E_a, m_a is the mass of the air removed from or introduced into the compartment, and R_a is the resistance. According to the Gay–Lusac law, E_a and m_a depend on the volume and the amount of air in the compartment. The volume-pressure dynamics are thus nonlinear. We model this nonlinearity through the scheduling of local linear models obtained at several operating points, defined by the current volume of the compartment V, the sleeve position x, and the absolute value of the flow rate $|F|$

$$\Theta = [x, V, |F|]^T.$$

Based on the above considerations, the transfer function from the volume change around the operating point to the pressure drop in the flow resistance $P_{\rm aw}$ is given by

$$G_{\rm PV}(s) = \frac{P_{\rm aw}(s)}{V(s)} = \frac{b_{1c}s}{s^2 + a_{1c}s + a_{0c}} \quad (18)$$

where the parameters b_{1c}, a_{1c}, and a_{0c} are specific to the given operating point Θ. Since we are interested in a discrete-time controller, $G_{\rm PV}$ is written in its discrete-time form, with the parameter dependence explicitly stated

$$G_{\rm PV}(q) = \frac{P_{\rm aw}(q)}{V(q)} = \frac{b_1(\Theta)(q-1)}{q^2 + a_1(\Theta)q + a_0(\Theta)}. \quad (19)$$

The parameters of the local models can be estimated by using standard linear identification techniques. Identification experiments were conducted with the volume excited around each operating point by using a pseudorandom binary signal. The corresponding pressure data $P_{\rm aw}$ were collected at a sampling rate of

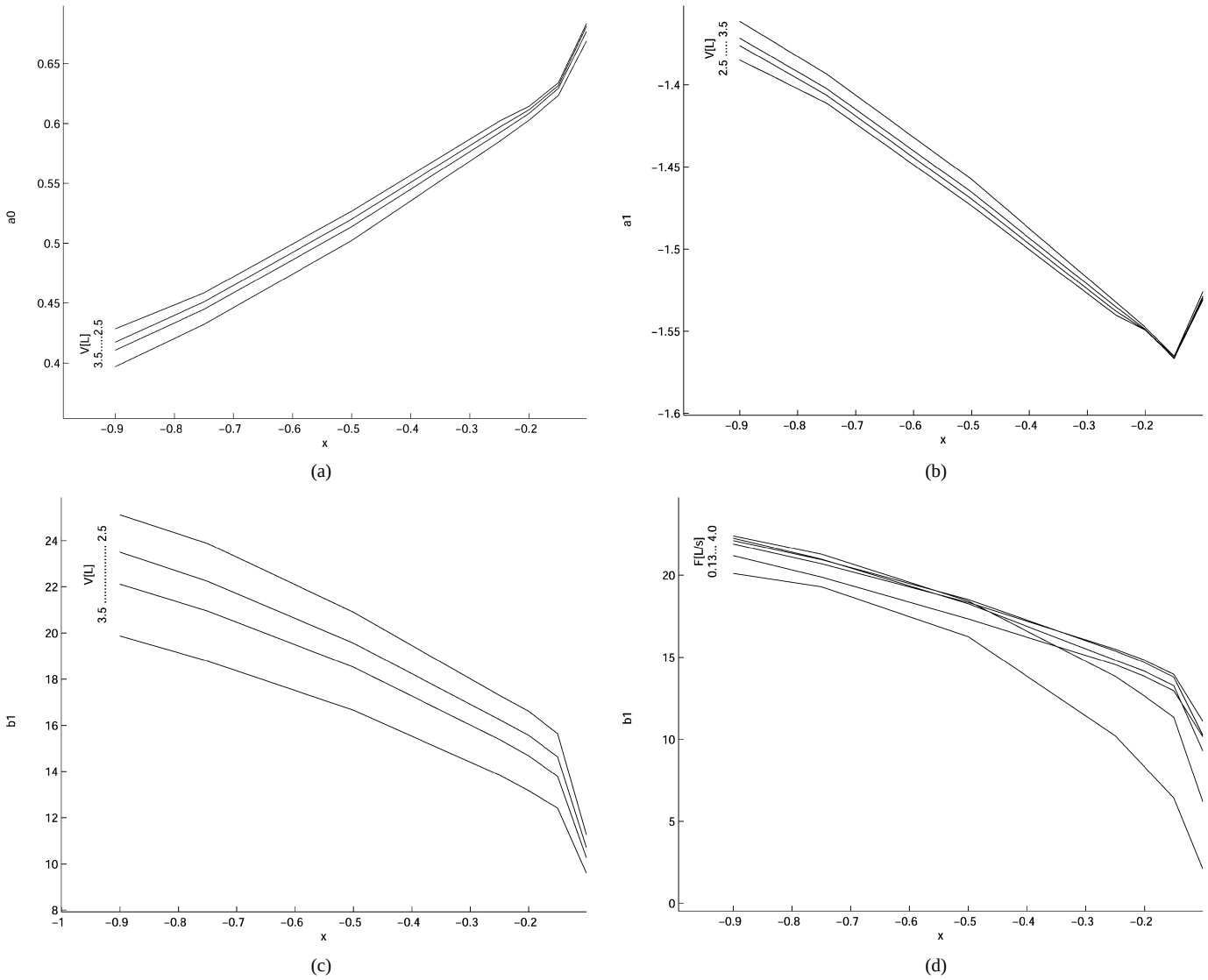

Fig. 11. Parameters a_0, a_1, and b_1 as functions of the scheduling variables.

200 Hz. During the identification experiment, the mouth pressure P_m was equal to zero (atmospheric pressure at the outlet) and from (15) we have $P_{\text{aw}} = -P_A$ (see also Fig. 1). Offsets and linear trends were first removed from the data and then the output error method [28] was used to obtain the parameters.

The operating points were chosen at a grid defined by three monotonically ordered vectors for the sleeve position $x_\Theta = [x_1, x_2, \ldots, x_{nx}]^T$, volume $V_\Theta = [V_1, V_2, \ldots, V_{nv}]^T$, and absolute flow rate $F_\Theta = [F_1, F_2, \ldots, F_{nf}]^T$. As the choice of the flow-rate operating points appeared to be crucial for good modeling performance, we optimized the entries of the flow vector F_Θ by the Levenberg–Marquardt method. The identified parameters $b_1(\Theta)$, $a_0(\Theta)$, and $a_1(\Theta)$ are stored in three-dimensional lookup tables and linear interpolation is used to obtain a smooth model.

Here, we illustrate the identification for four different volumes ($V_\Theta = [2.5, 2.7, 3.0, 3.5]^T$) and six different sleeve positions ($x_\Theta = [-0.90, -0.75, -0.50, -0.20, -0.15, -0.10]^T$). These operating points were chosen by examining the nonlinearities that originate from the Gay–Lusac law and the mechanical construction of the flow resistance. Five different amplitudes of the random binary volume reference signal were used. The choice of the amplitudes was based on the flows expected in the mechanical simulation. The initial absolute flow vector was $F_\Theta = [0.05, 0.25, 0.40, 0.97, 1.50]^T$ and the optimized absolute flow vector obtained through data fitting was $F_\Theta = [0.13, 0.45, 0.73, 1.04, 4.00]^T$. Table II illustrates the modeling accuracy achieved at the different operating points. The model performance is measured by means of the *variance accounted for* (VAF) index, defined by

$$\text{VAF} = 100\% \cdot \left[1 - \frac{\text{var}(P_{\text{aw}} - P_{\text{aws}})}{\text{var}(P_{\text{aw}})}\right] \tag{20}$$

where P_{aws} is the pressure simulated by using G_{PV} and P_{aw} is the pressure measured in the lung simulator. One can see that at high resistance values and large volumes, the modeling accuracy is better.

To illustrate the nonlinearity of the identified model, Fig. 11 shows the scheduled parameters a_0, a_1, b_1 as a function of the volume V and the sleeve position x, and the parameter b_1 as a function of the absolute flow $|F|$ and the sleeve position x.

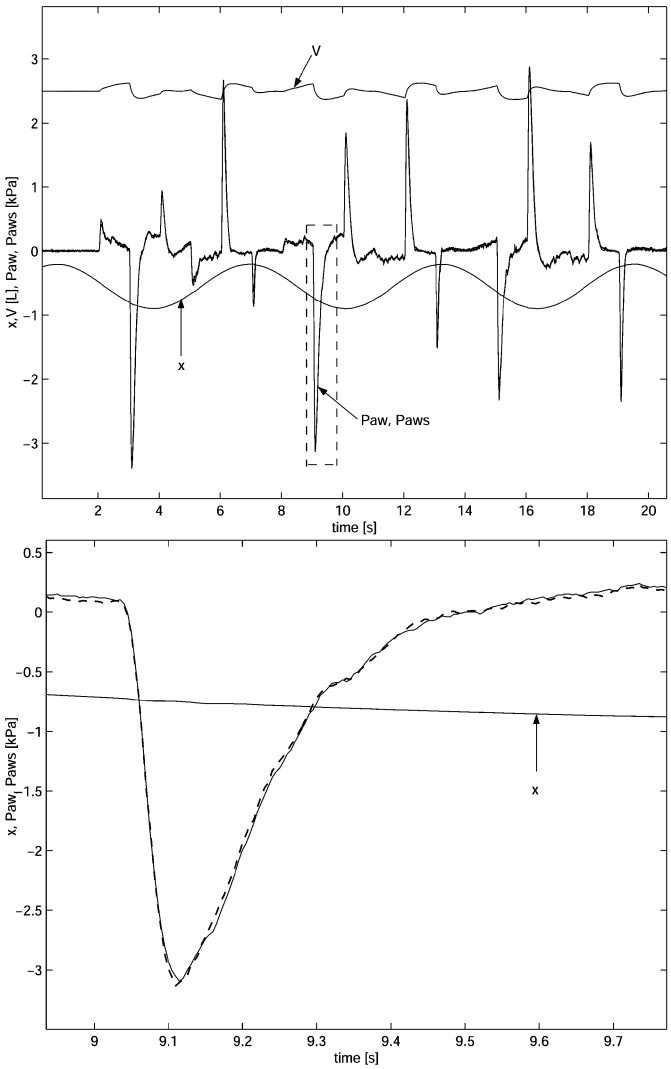

Fig. 12. Top: measured P_{aw} and simulated P_{aws} for different sleeve positions x and volumes V. Bottom: a close-up of the selected region in the top figure (P_{aw}—solid; P_{aws}—dashed).

A comparison of the measured P_{aw} and the simulated P_{aws} is shown in Fig. 12. The input signal was a binary random signal applied to the volume reference. We can conclude that the model is in a reasonable agreement with the measured data.

V. Control Design

The control system has been designed to achieve the desired compliance properties, nonlinearities, volume, and flow-dependent characteristics. It also has to compensate for parasitic phenomena such as time delays in the control loops and (undesired) nonlinearities of the simulator itself. In this section, the design of high-level controllers for the flow resistor and for the piston position (volume) is addressed.

A. Flow Resistance

The task of this controller is to determine the sleeve position reference x_{ref} for the low-level sleeve-position control loop, which has been discussed in Section IV-A. This is accomplished by inverting the static nonlinearity $R = f(x, F)$, defined by the lookup table shown in Fig. 8. Note that at a constant flow rate

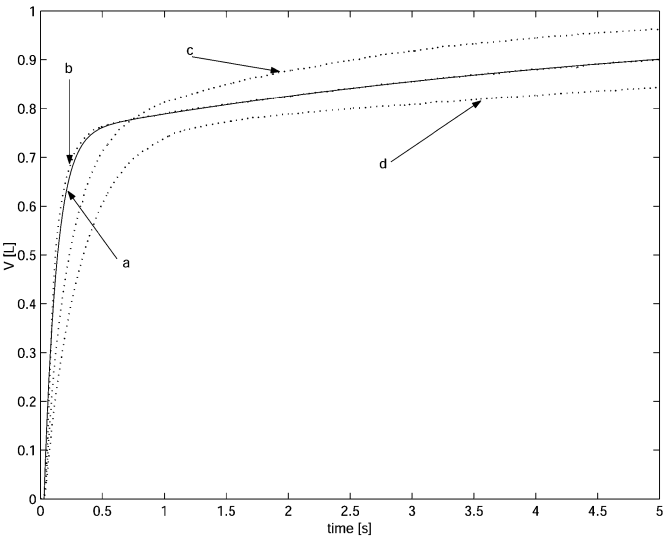

Fig. 13. Measured (dotted line) and simulated (solid line) step responses of the volume control loop. (a) $\tau_1 = 0.1$ s and (b) $\tau_2 = 5.27$ s. (c) $\tau_1 = 0.25$ s and $\tau_2 = 2.5$ s. (d) $\tau_1 = 0.5$ s and $\tau_2 = 10$ s.

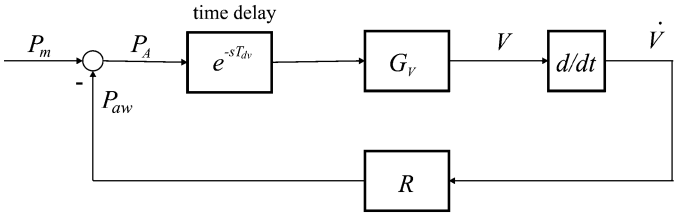

Fig. 14. Linearized version of the model given in Fig. 5.

F, the flow resistance monotonically decreases with the sleeve position x (due to a smaller active resistance region). At a constant sleeve position x, the flow resistance increases with the absolute value of the flow rate $|F|$ (due to turbulence). As the overall relation is monotonic, it is possible to calculate an inverse lookup table (by means of linear interpolation), which relates the desired resistance R_{ref} and the current flow rate F to the reference sleeve position x_{ref}

$$x_{\mathrm{ref}} = f^{-1}(R_{\mathrm{ref}}, F).$$

The desired resistance R_{ref} is computed by using the resistance model (14). As the true flow rate is measured, the theoretical derivative $\dot{V}$ can be replaced by the measured value F, which yields

$$R_{\mathrm{ref}} = R_0 + K_V V + K_F |F|. \tag{21}$$

B. Volume Control

In order to obtain the desired dynamic compliance, the volume reference is computed from the measured P_A by using the viscoelastic model (11) in series with a prefilter $0.1s + 1$ that compensates for the dominant DMC dynamics (see Section IV-B)

$$G_{cV}(s) = \frac{V_{\mathrm{ref}}(s)}{P_A(s)} = \frac{0.1s+1}{E}\left(\frac{K_1}{\tau_1 s+1} + \frac{1-K_1}{\tau_2 s+1}\right). \tag{22}$$

The values of K_1 and τ_2 were determined as described in Section III. This transfer function has been implemented in

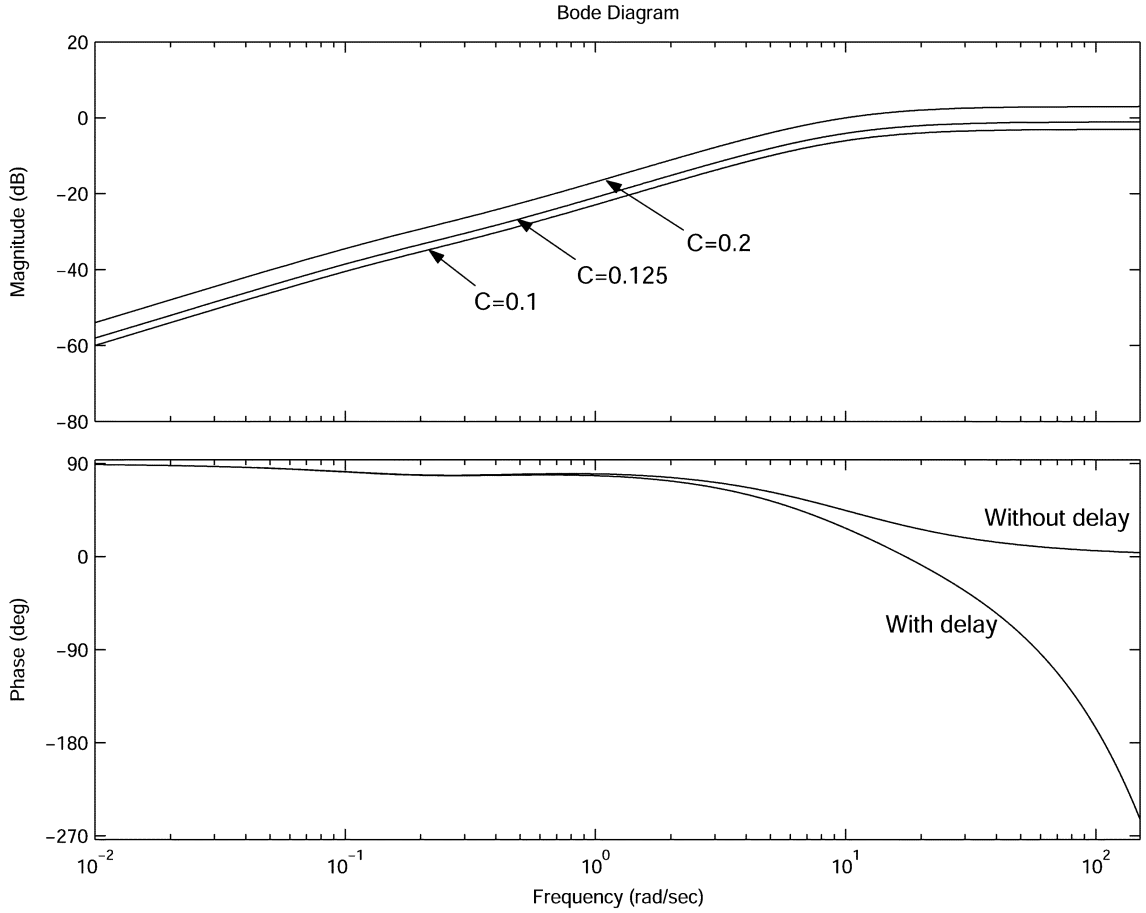

Fig. 15. Bode diagram of G_o for parameter values $\tau_1 = 0.1$ s, $\tau_2 = 5.27$ s, $R = 1$ kPasl^{-1}, $K_1 = 0.7$, and $T_{dv} = 0.03$ s.

MATLAB/Simulink. Fig. 13 shows a comparison of measured and simulated step responses of the volume control loop for a step of $P_A = 1$ kPa with the following parameters: $C = 1$ lkPa^{-1}, $K_1 = 0.74$, $\tau_2 = 5.27$ s, and $\tau_1 = 0.1$ s. One can see that the measured and simulated responses are in a good agreement [Fig. 13(a) and (b)]. Responses [Fig. 13(c) and (d)] illustrate the behavior for different values of τ_1 and τ_2.

From (22), one can see that the measured pressure P_A is used to determine the reference for the piston position. The motion of the piston in turn influences the pressure. In this way, a closed-loop system is introduced (see also Fig. 5), whose stability must be analyzed, taking into account the time delay in (17).

Fig. 14 shows a linearization of the model given in Fig. 5, in which the nonlinear resistance has been replaced by a constant resistance value R and the time delay T_{dv} of the piston-position control loop (17) has been added. The influence of the time delay on the stability of the closed loop can be analyzed in the Bode diagram of the open-loop transfer function

$$G_o(s) = s\frac{R}{E}\left(\frac{K_1}{s\tau_1+1} + \frac{1-K_1}{s\tau_2+1}\right)e^{-sT_{dv}}. \qquad (23)$$

This plot is given in Fig. 15 for realistic parameter values $\tau_1 = 0.1$ s, $\tau_2 = 5.27$ s, $R = 1$ kPasl^{-1}, $K_1 = 0.7$, and $T_{dv} = 0.03$ s. One can see that when the compliance increases, the closed loop becomes unstable (the gain is greater than 0 dB at a phase shift of 180°). This is due to the extra phase shift introduced by the time delay. Note that without the time delay, the closed-loop system is always stable, regardless of the compliance value.

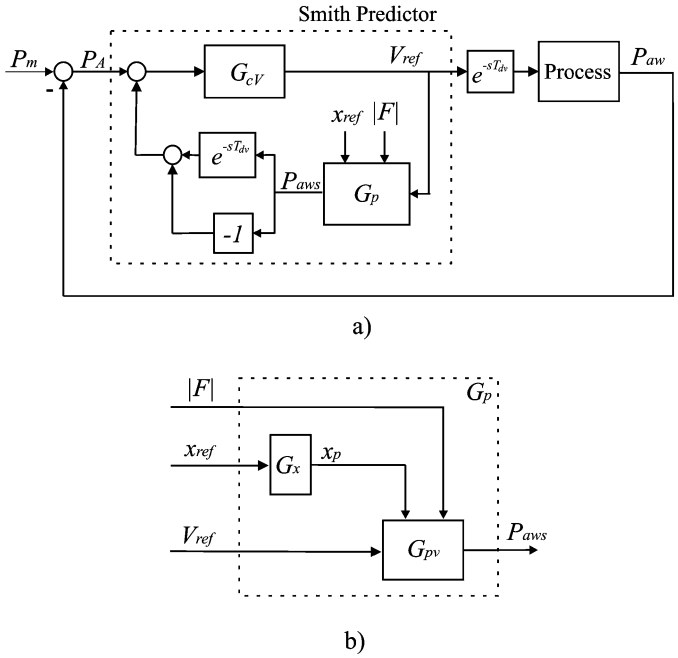

Fig. 16. (a) Smith predictor. (b) Model of the process G_p.

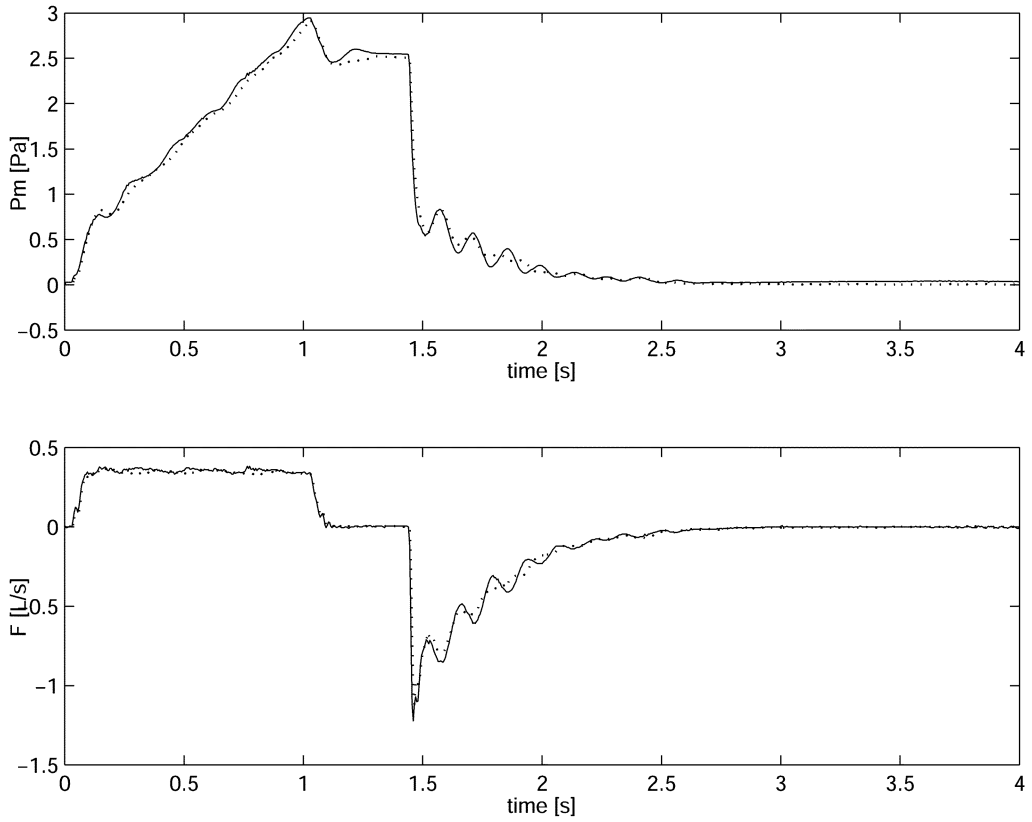

Fig. 17. Real-time simulation results: mouth pressure and flow measured in the simulator with the Smith predictor (dotted line) and without it (solid line).

To compensate for the time delay, we make use of the Smith-predictor control scheme [29], given in Fig. 16. In the controller, a delay-free model of the process "predicts" the output over the period of this delay. To this end, an accurate model of the process dynamics is needed. Here, we use the discrete-time models identified in Section IV. Note that the delay-free transfer functions $G_x(q)$ and $G_{\mathrm{DMC}}(q)$ are employed, see (16) and (17).

C. Real-Time Validation

This section presents experimental results obtained on the mechanical simulator. The servo ventilator ("SERVO VENTILATOR" 900, Siemens Elema, Sweden) was connected to the simulator. The ventilator was programmed for 6 L per min and 15 breaths per min with the inspiration time 25%, pause time 10%, and PEEP $= 0$. The parameter values of the lung model to be simulated were: $C = 0.1$ lkPa^{-1}, $\tau_1 = 0.1$ s, and $K_1 = 1$. The sleeve position was kept constant at $x_{\mathrm{ref}} = 0.5$.

Fig. 17 shows the mouth pressure and the flow signals measured in the lung simulator with the Smith predictor (dotted line) and without it (solid line). One can see that the Smith predictor reduces the oscillations, but it does not suppress them completely. There are several reasons for this. First, the sample rate of the discrete-time controller is not sufficiently high and, thus, it does not allow for an accurate representation of the time delay in terms of multiples of the sampling period. A higher sampling rate cannot be used because of the hardware/software limitations of the current setup. Secondly, a closer examination reveals that the models G_v, G_x, and G_{PV} are not sufficiently accurate, see, e.g., Fig. 12. Finally, the ventilator may have some influence on the simulator dynamics as it is not an ideal pressure source. This could be prevented by using the measured pressure P_m in the controller.

VI. Conclusion

A new approach to mechanical simulation of lung behavior has been introduced that uses a computer-controlled active mechatronic system. A nonlinear single-compartment mathematical model of the artificially ventilated respiratory system has been derived and incorporated into the simulator control system. This model can capture both static and dynamic compliance of the respiratory system and nonlinear flow-resistance properties. Parameters in this model can be estimated by using data from artificially ventilated patients. It is shown that the simulation model fits patient data well. To simulate a broader spectrum of pulmonary pathologies, the model can be extended in a rather straightforward manner, by incorporating, e.g., higher order models of the dynamic compliance, flow limitation, dynamic hyperventilation, airways compression, inspiratory, or expiratory triggering, etc. The effects of heart activity can also be simulated by adding this influence to the volume change due to the already modeled mechanical lung properties.

The model of the respiratory system was then matched to a model of the available physical equipment (the simulator, the actuators, and the interface electronics) in order to obtain the desired lung behavior. A significant time delay in the piston motion control loop was identified. While this delay has no negative effects in the simulation of active breathing, it causes os-

cillations when simulating an artificially ventilated respiratory system. This is especially the case for high compliance values and fast dynamic changes. A controller based on the Smith-predictor scheme was developed to control the piston motion by using feedback from the pressure sensor. However, the effectiveness of this scheme is limited by the modeling errors and the available computing power. Although advanced system identification techniques were applied, the nonlinear nature of the process makes the modeling difficult. One possible approach to solving this problem is to redesign the equipment and replace the screw that drives the piston by a more compliant transmission. One can think of a linear electrical servo, for instance. Then, the compartment pressure would directly act on the electrical actuator as a disturbance force. By controlling the actuator through state feedback, the desired compliant behavior could be achieved. As a result, the effect of time delays would be minimal.

The importance of a reliable and flexible mechanical lung simulator will gradually increase. We incorporated in the simulator several aspects of lung behavior as described in literature (viscoelasticity, flow-dependent resistance, and volume-dependent lung compliance). In this way, different aspects of lung pathology and their influence on signals measured on ventilated patients can be simulated and presented to, e.g., doctors and nurses in a simulation environment in order to train their skills to perceive such phenomena in a real patient situation. Through simulation in a realistic situation the possibilities and limitations of analysis techniques can be demonstrated and the acceptance of new techniques in an intensive-care unit can be facilitated. The lung simulator will also be of importance for device testing, where a physical model is required for optimal model-machine interaction. The incorporation of active inspiratory and expiratory triggering will be one of the goals of our future research. In this way, the triggering mode of the ventilators can be studied in order to improve the patient-ventilator interaction, which is a topic that has not been satisfactorily addressed in the current literature.

ACKNOWLEDGMENT

The authors wish to thank D. Butterman and M. J. Nieman for their editorial suggestions.

REFERENCES

[1] E. Salazar and J. H. Knowles, "An analysis of pressure-volume characteristics of the lungs," *J. Appl. Phys. Respir. Envir. Excer. Phys.*, vol. 19, pp. 97–104, 1964.
[2] T. Similowski and J. H. T. Bates, "Two-compartment modeling of respiratory system mechanics at low frequencies: gas redistribution or tissue rheology?," *Eur. Respir. J.*, vol. 4, pp. 353–358, 1991.
[3] W. Flugge, *Viscoelasticity*. New York: Springer-Verlag, 1975.
[4] J. B. West, *Bioengineering Aspects of the Lung, Lung Biology in Health and Disease*. New York: Marcel Dekker, 1977.
[5] A. F. M. Verbraak, J. M. Bogaard, J. E. W. Beneken, E. Hoorn, and A. Versprille, "Serial lung model for simulation and parameterestimation in body plethysmography," *Med. Biol. Eng. Comput.*, vol. 29, pp. 309–317, 1991.
[6] J. M. Bogaard, W. Jonker, A. F. M. Verbraak, and A. Versprille, "A simplified procedure for exponential fitting of pressure-volume curves of normal and diseased lungs," *Respiration*, vol. 49, pp. 181–186, 1986.
[7] R. Peslin, J. Felicio da Silva, F. Chabot, and C. Duvivier, "Respiratory mechanics studied by multiple linear regression in unsedated ventilated patients," *Eur. Resp. J.*, vol. 5, pp. 871–879, 1992.
[8] (1994) DMC-1000 Technical Reference Guide V. 1.3. Galil Motion Control, Inc.. [Online]http://www.galilmc.com/catalog/catoptima.pdf
[9] A. F. M. Verbraak, W. Holland, B. Mulder, J. M. Bogaard, and A. Versprille, "Computer-controlled flow resistance," *Med. Biol. Eng. Comput.*, vol. 39, no. 1, pp. 770–775, 1999.
[10] A. F. M. Verbraak, P. R. Rijnbeek, J. E. Beneken, J. M. Boogaard, and A. Versprille, "A new approach to mechanical simulation of lung behavior: pressure-controlled and time-related piston movement," *Med. Biol. Eng. Comput.*, vol. 39, no. 1, pp. 82–89, 2000.
[11] "PCL 812PG Manual," Advantech Co., 1995.
[12] R. Rhoades and R. Pflanzer, *Human Physiology*, 2nd ed. Philadelphia, PA: Saunders, 1992.
[13] R. N. Elaine Marieb, *Human Anatomy & Physiology*, 4th ed. Reading, MA: Addison-Wesley, 1998.
[14] A. T. Johnson and J. D. Bronzino, "Respiratory system," in *The Biomedical Engineering Handbook*, J. D. Bronzino, Ed. Boca Raton, FL: CRC, 1995, pp. 70–86.
[15] B. Suki, "Nonlinear phenomena in respiratory mechanical measurements," *J. Appl. Phys.*, vol. 74, no. 5, pp. 2574–2584, 1993.
[16] W. C. Burke, P. S. Crokke, T. W. Marcy, A. B. Adams, and J. J. Marini, "Comparison of mathematical and mechanical models of pressure-controlled ventilation," *J. Appl. Phys.*, vol. 74, no. 2, pp. 922–933, 1993.
[17] J. H. T. Bates, A. Rossi, and J. Milic-Emili, "Analysis of the behavior of the respiratory system with constant inspiratory flow," *J. Appl. Phys.*, vol. 58, pp. 1840–1848, 1985.
[18] J. Mead and E. Agostoni, "Dynamics of breathing," in *Handbook of Physiology, Respiration*, W. O. Fenn and H. Rahn, Eds., 1964, vol. 1, pp. 411–427.
[19] R. M. Corless, G. H. Gonnet, D. E. G. Hare, D. J. Jeffrey, and D. E. Knuth, "On the Lambert W function," *Adv. Comput. Math.*, vol. 5, pp. 329–359, 1996.
[20] F. G. Hoppin and J. Hildebrandt, *Mechanical Properties of the Lung*. New York: Marcel Dekker, 1997.
[21] J. T. Sharp, F. N. Johnson, N. B. Goldberg, and P. Van Lith, "Hystheresis and stress adaptation in the human respiratory system," *J. Appl. Phys.*, vol. 23, pp. 487–497, 1989.
[22] J. Hildebrandt, "Pressure-volume data of cat lung interpreted by a plastoelastic, linear viscoelastic model," *J. Appl. Phys.*, vol. 28, pp. 365–372, 1970.
[23] C. D. Stamenovic, G. M. Glass, G. M. Barnas, and J. J. Fedberg, "A model of imperfect elasticity of the human chest wall," *The Physiologist*, vol. 31, p. A220, 1988.
[24] F. H. D. Patton, A. F. Fuchs, B. Hille, A. M. Scher, and R. Steiner, *Textbook of Physiology*. St. Louis, MO: Mosby, 1988.
[25] R. Babuška, L. Alic, M. S. Lourens, A. F. M. Verbraak, and J. Bogaard, "Estimation of respiratory parameters via fuzzy clustering," *Artif. Intell. Medicine*, vol. 21, no. 1–3, pp. 91–105, 2001.
[26] K. Levenberg, "A method for the solution of certain problems least-squares," *Q. Appl. Math.*, vol. 2, p. 164, 1944.
[27] D. Marquardt, "An algorithm for the least-squares estimation of nonlinear parameters," *SIAM J. Appl. Math.*, vol. 11, p. 431, 1963.
[28] L. Ljung and T. Glad, *Modeling of Dynamic Systems*. Englewood Cliffs, NJ: Prentice-Hall, 1994.
[29] K. Astrom and B. Wittenmark, *Computer Controlled Systems*. Englewood Cliffs, NJ: Prentice-Hall, 1977.

Samir Mešić was born in Ševarlije, Bosnia and Hercegovina, in 1970. He received the B.Sc. degree from the University of J. J. Strossmayer, Osijek, Croatia, in 1998. He received the M.Sc. degree from the Delft University of Technology, The Netherlands, in 2001. Since March 2002 he has been pursuing the Ph.D. degree in control systems engineering at Delft Center for Systems and Control, Delft University of Technology.

His Ph.D. degree project is focused on fault detection and isolation, fault tolerant control, and the application of these techniques to relevant industrial problems. His other research interests are biomedical engineering and image processing.

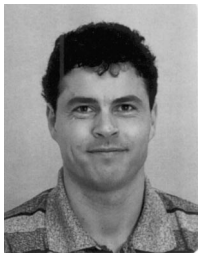

Robert Babuška received the M.Sc. degree in control engineering from the Czech Technical University in Prague, Czechoslovakia, in 1990, and the Ph.D. degree from the Delft University of Technology, The Netherlands, in 1997.

Currently, he is a Professor at the Delft Center for Systems and Control, Faculty of Mechanical Engineering, Delft University of Technology. He has coauthored more than 50 journal papers and chapters in books and has published a research monograph *Fuzzy Modeling for Control* (Norwell, MA: Kluwer, 1998). He is serving as an Area Editor of *Fuzzy Sets and Systems*, and Associate Editor of *Engineering Applications of Artificial Intelligence*. His research interests include the use of fuzzy set techniques and neural networks in nonlinear system identification and control.

Dr. Babuška is serving as an Associate Editor of the IEEE TRANSACTIONS ON FUZZY SYSTEMS. He is the Chairman of the IFAC technical committee on Cognition and Control.

Henk C. Hoogsteden received the M.D. degree from the State University of Groningen, The Netherlands, and the Ph.D. degree from the Erasmus University, Rotterdam, The Netherlands.

Currently, he is a Professor of pulmonary medicine and Head of the Pulmonary and Critical Care Department at Erasmus University Medical Center, Rotterdam, The Netherlands. He is the author of more than 120 papers focusing on the immunological basis of pulmonary diseases.

Anton F. M. Verbraak received the M.S. degree at the Eindhoven University of Technology, The Netherlands, and the Ph.D. degree at the Medical Faculty of the Erasmus University, Rotterdam, The Netherlands.

Currently, he is a Clinical Physicist in the Department of Pulmonary Medicine, Erasmus University Medical Center, Rotterdam, The Netherlands. His fields of interest are signal processing, physiological modeling, simulation and control with emphasis on respiratory mechanics, pulmonary function, artificial ventilation, and intensive care.

Dr. Verbraak is the Treasurer of the Dutch Society for Biophysics & Biomedical Technology and the Chairman of the Biomedical Technology Section.